Available online at www.sciencedirect.com
SCIENCE DIRECT®
Engineering Fracture Mechanics 72 (2005) 2009–2017
Engineering Fracture Mechanics
www.elsevier.com/locate/engfracmech

Computational simulations of intergranular fracture of polycrystalline materials and size effect

J.-R. Li, J.-L. Yu *

CAS Key Laboratory of Mechanical Behavior and Design of Materials, University of Science and Technology of China, Hefei 230026, China

Received 27 January 2004; received in revised form 15 September 2004; accepted 17 October 2004
Available online 2 March 2005

Abstract

Grain boundaries are important elements associated with micro-structural heterogeneity in polycrystalline materials. The influence of the grain boundary character distribution on intergranular fracture of polycrystals is investigated in this paper. Considering the random heterogeneity of materials, a two-dimensional stochastic finite element method (SFEM) is used to simulate the intergranular damage and failure process of polycrystals. The impact of the fraction and distribution of random grain boundaries on the fracture behavior is discussed, and the effect of model size on results is also evaluated.

1. Introduction

Grain boundaries and interphase boundaries strongly affect the mechanical properties in polycrystalline materials. The Hall–Petch effect is a well-known example. Intergranular brittleness is another detrimental effect of grain boundaries on mechanical properties. Grain boundaries can be preferential sites for crack nucleation and propagation.

Based on the coincident-site lattice model (CSL), grain boundaries can be geometrically described by a parameter, Σ, a measure of the reciprocal density of coincident lattice sites. It has been found that the propensity for intergranular fracture is closely related to the type and structure of grain boundaries. Low angle boundaries and certain special boundaries with $\Sigma < 29$ are found to confer high resistance to intergranular fracture [1]. Therefore, $\Sigma < 29$ boundaries can be referred as special boundaries and $\Sigma > 29$ as random

* Corresponding author. Tel.: +86 551 3603793; fax: +86 551 3606459.
E-mail address: jlyu@ustc.edu.cn (J.-L. Yu).

0013-7944/$ - see front matter © 2005 Elsevier Ltd. All rights reserved.
doi:10.1016/j.engfracmech.2004.10.016

boundaries. The optimization of the grain boundary character distribution (GBCD) and the grain boundary connectivity are a key to produce desirable bulk mechanical properties in both structural and functional polycrystalline materials [2].

In this paper, a micro-mechanical stochastic finite element method is used to model the intergranular micro-crack initiation and evolution in polycrystalline micro-structures. The heterogeneity and grain boundary character distribution are considered. Cohesive interface elements are embedded along grain boundaries to simulate initiation and evolution of micro-cracks.

2. Computational model

We shall focus on the fraction and distribution of random grain boundaries and their effect on the intergranular fracture. The material data for aluminum polycrystal are taken as an example in the model, though it is not a typical material for grain boundary engineering because of its relatively lower faction of special grain boundaries. The stiffness data of aluminum single crystal are taken from Ref. [3] that

$$C_{11} = 108.2\ \text{GPa}, \quad C_{12} = 61.3\ \text{GPa}, \quad C_{44} = 28.5\ \text{GPa}, \quad 2C_{44}/(C_{11} - C_{12}) = 1.22$$

where the last parameter, $2C_{44}/(C_{11} - C_{12})$, describes its elastic anisotropy. Single crystal of aluminum shows little elastic anisotropy.

The crystal-plasticity-based computational micro-mechanic models can offer better prediction of the local deformation and texture evolution in polycrystals than continuum elastic–plastic theory [4]. As our interest is the intergranular fracture, the following continuum elastic–plastic stress–strain relationship of individual grain is adopted [5],

$$\sigma = \begin{cases} E\varepsilon & (\varepsilon \leqslant \varepsilon_0^e) \\ \sigma_0^e + E'(\varepsilon - \varepsilon_0^e) & (\varepsilon_0^e < \varepsilon \leqslant \varepsilon_{01}^e) \\ \sigma_{01}^e + k(\varepsilon - \varepsilon_{01}^e)^{1/2} & (\varepsilon_{01}^e < \varepsilon) \end{cases} \tag{1}$$

where ε_0 and σ_0 are the equivalent yielding strain and stress, respectively, E' is the hardening coefficient in stage I, ε_{01} and σ_{01} are the equivalent strain and stress, respectively, when stage I is finished, and k is a material parameter.

A multi-body contact-interface algorithm describing the kinematics at the grain boundaries is used to simulate crack initiation and propagation. A cohesive zone model through a so-called "spot welds" in the ABAQUS code [6] is employed to simulate the intergranular cracking. It is assumed that a spot weld carries a force normal to the surface onto which the node is welded, F^{n}, and a shear force tangent to the surface, F^{s}. Once failure is detected, the weld constraint is relaxed linearly over a time period T_{f}. Hence the failure initiation and post-failure behavior of a spot weld is described by,

$$\left(\frac{\max(F^{\text{n}}, 0)}{F_{\text{f}}^{\text{n}}}\right)^2 + \left(\frac{F^{\text{s}}}{F_{\text{f}}^{\text{s}}}\right)^2 = \left(1.0 - \frac{t}{T_{\text{f}}}\right)^2 \tag{2}$$

where F_{f}^{n} is the force required to cause failure in tension, F_{f}^{s} the force required to cause failure in pure shear, and t the time since the initial failure of the weld is detected. If the normal force is compressive, it is replaced by zero in Eq. (2).

Eq. (2) can be converted into stress and strain description as:

$$\left(\frac{\max(\sigma^{\text{n}}, 0)}{\sigma_{\text{cr}}^{\text{n}}}\right)^2 + \left(\frac{\sigma^{\text{s}}}{\sigma_{\text{cr}}^{\text{s}}}\right)^2 \leqslant \left(1.0 - \frac{\Delta\varepsilon}{c}\right)^2 \tag{3}$$

where, σ^n and σ^s are the normal stress and shear stress of the grain boundary, σ^n_{cr} and σ^s_{cr} are the tensile and shear strengths, respectively, $\Delta\varepsilon$ is the strain increment, and c a parameter related to the ductility of the material. This fracture criterion is a special case of the linear cohesive zone model proposed by Camacho and Ortiz [7] (1996) with the boundary friction coefficient of zero.

Pure aluminum with coarse grain size of about 2 mm is chosen, and its macroscopic yield stress is 17.4 MPa. The strength of the random grain boundaries is much lower than that of the special grain boundaries and varies with the disorientation angle. In this study, we just simply designate two pairs of strengths, $\sigma^n_{cr} = 14$ MPa, $\sigma^s_{cr} = 7$ MPa, and $\sigma^n_{cr} = 28$ MPa, $\sigma^s_{cr} = 14$ MPa, for random grain boundaries and special grain boundaries, respectively.

The finite element models are shown in Fig. 1. Different grain orientation and finite deformation are considered. A calculation program is used to generate a random grain number list, and correlated material properties are endued to the elements according to the list. Thus a random sample of grain distribution

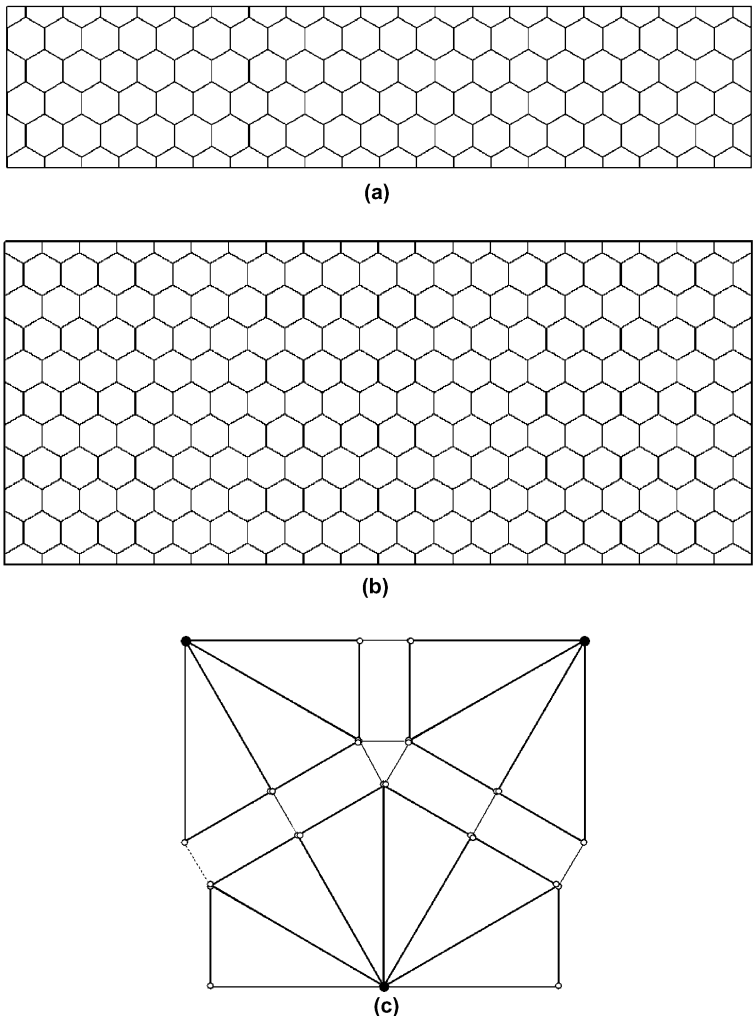

Fig. 1. Polycrystal models: (a) a narrow band with width of 7.5 mm, (b) a wide band with width of 15.0 mm, their lengths are both 34.64 mm, and (c) the interface elements in grain boundaries.

can be obtained. Similarly, grain boundaries are also randomized. Some grain boundaries are selected as random grain boundaries with weak strength. Fifty sets of different random grain boundary distributions for the narrow band model are calculated. Each set consists samples with increasing number of random grain boundaries generated from one set of random numbers.

3. Results and discussion

Fig. 2 shows the variation of the fracture energy, $G_f = \int_0^{\varepsilon_f} \sigma \, d\varepsilon$, and the fracture strain of a typical set of samples with the increase of the distributed random grain boundaries for the narrow band model. It is evident that the variation of the two curves can be described into three stages. In the initial stage, with the increase of the random grain boundaries, the material performance degrades quickly. Then, in the second stage, the fracture energy increases a little higher than that at the end of the first stage, though it is still changing with the random grain boundary fraction. The fracture strain in the second stage is much large. Finally, when the random grain boundaries are largely distributed, the fracture energy is much low and changes very little with the variation of the random grain boundary fraction.

The results of the total 50 sets of samples are statistically analyzed. The variations of the averaged fracture energy and fracture strain with the random grain boundary fraction and their mean square deviations

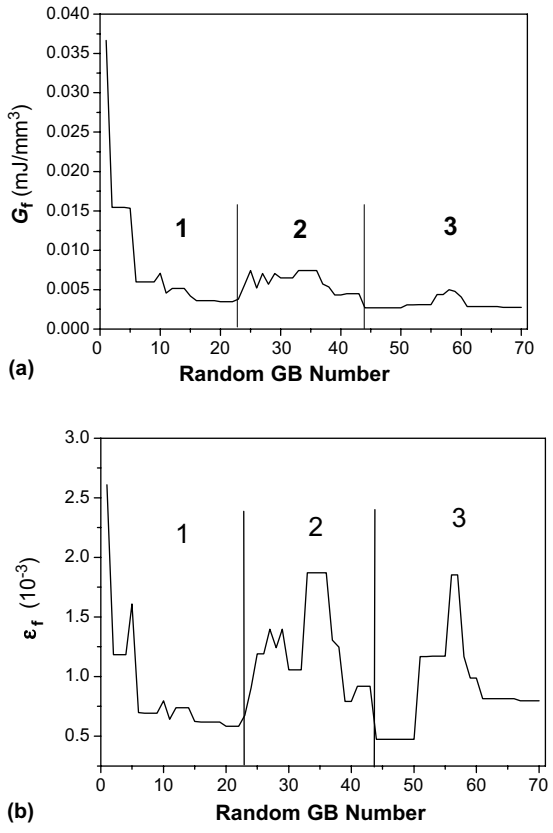

Fig. 2. Variations of (a) fracture energy and (b) fracture strain with the random grain boundary number.

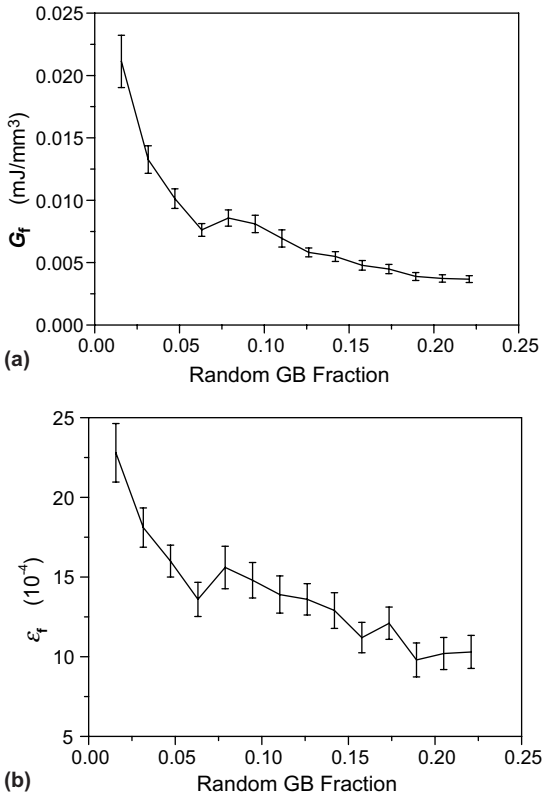

Fig. 3. Variation of (a) statistic fracture energy, and (b) fracture strain with the random grain boundary fraction of the narrow band model.

are shown in Fig. 3. It transpires that the fracture energy does not decrease monotonously with the increase of the random grain boundary fraction. A stage with certain increase of fracture energy exists, indicating some toughening effect of increasing random grain boundaries.

Both the individual and statistical results indicate the toughening effect, i.e., the increase of random grain boundaries in some range will enhance the fracture performance of the polycrystals. We analyze the toughening effect of random grain boundary in detail. Two toughening phenomena are found. Fig. 4 shows the two random grain boundary distributions. In Fig. 4a, 20 random grain boundaries are distributed, called sample A, while in Fig. 4b; 10 random grain boundaries are added based on Fig. 4a, called sample B. Fig. 5a and b show the final fracture grain boundaries of samples A and B. The main failure paths of the samples A and B are almost the same, whilst additional fracture grain boundaries in the main path of sample B is found when compared with that of sample A. Fig. 6 shows the nominal stress–strain curves of the two samples. Sample B exhibits better fracture performance than sample A. This toughening phenomenon may be caused by the bifurcation of main failure path due to added random grain boundaries.

Fig. 7 shows the other two random grain boundary distributions. In Fig. 7a, 20 random grain boundaries are distributed, called sample C, while in Fig. 7b; 10 random grain boundaries are added based on Fig. 7a, called sample D. Fig. 8a and b show the final fracture grain boundaries of the samples C and D. The main failure paths of the samples C and D are different and the main path length of sample C is

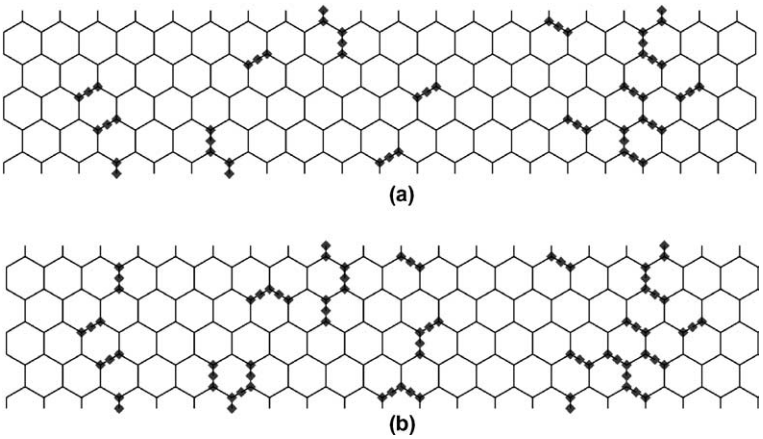

Fig. 4. Sequent random grain boundary distributions with (a) 20 random grain boundaries, sample A, and (b) 30 random grain boundaries, sample B.

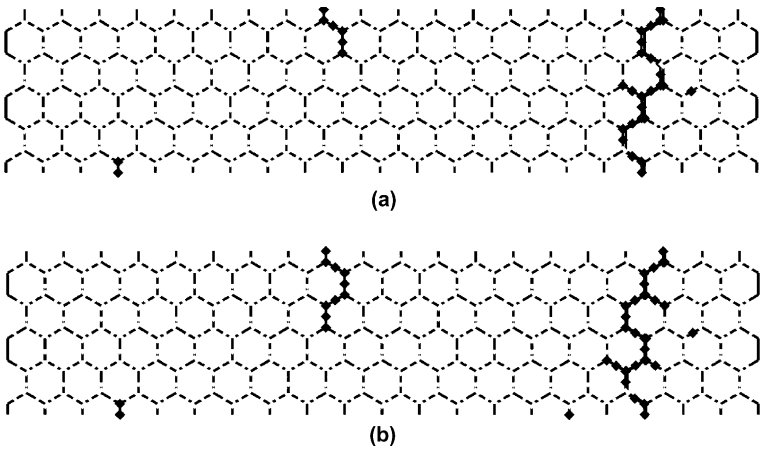

Fig. 5. Final fractured grain boundaries in (a) the sample A with 20 random grain boundaries and (b) the sample B with 30 random grain boundaries.

a little longer than that of sample D, whilst the individual fracture grain boundaries of sample D are more than that of sample C. Fig. 9 shows the nominal stress–strain curves of the two samples. Sample D exhibits better fracture performance than sample C. This toughening phenomenon may be caused by the rise of micro-damages due to added random grain boundaries.

Fig. 10 shows the variation of the fracture energy of a typical set of samples with the increase of the distributed random grain boundaries for the wide band model, in comparison with the narrow band model. The results are similar. However, the fracture energy of the wide band model is much higher than that of the narrow band model at the same random grain boundary fractions, indicating certain size effect. The reason is that the random grain boundaries can easily link up in the narrow band, and the fracture behavior is mostly related to the local weak paths.

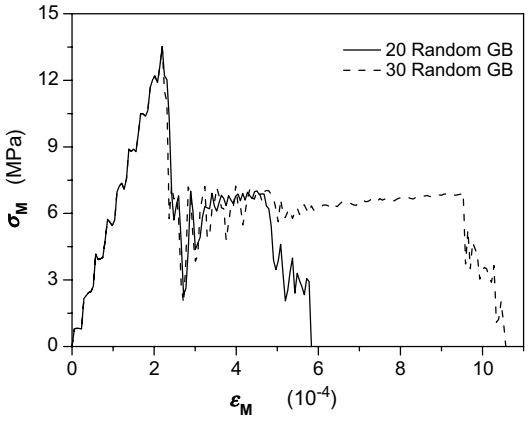

Fig. 6. The nominal stress–strain curves of the samples A and B.

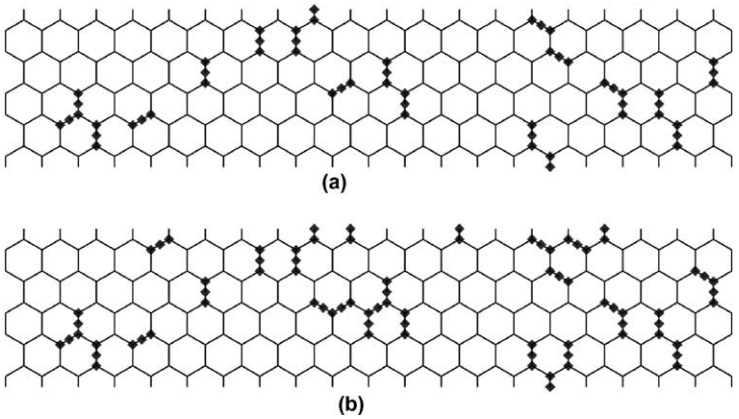

Fig. 7. Sequent random grain boundary distributions with (a) 20 random grain boundaries, sample C, and (b) 30 random grain boundaries, sample D.

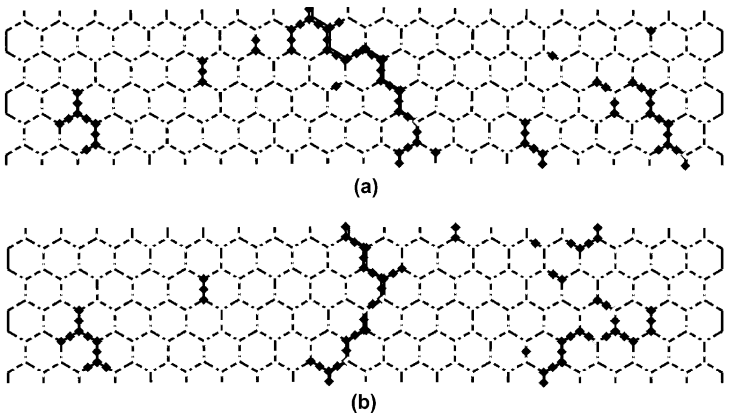

Fig. 8. Final fractured grain boundaries in (a) the sample C with 20 random grain boundaries and (b) the sample D with 30 random grain boundaries.

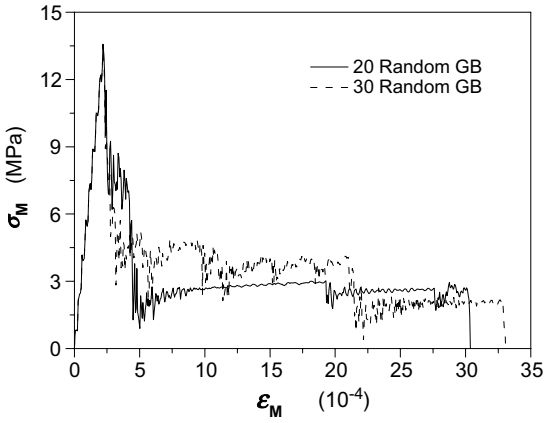

Fig. 9. The nominal stress–strain curves of the samples C and D.

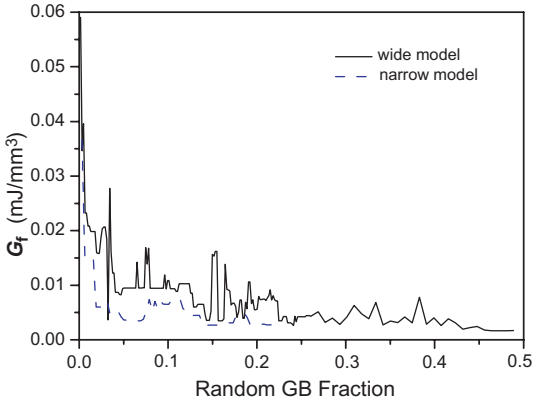

Fig. 10. Variation of fracture energy with the random grain boundary fraction of two models.

4. Conclusion

The damage process of metallic polycrystals is simulated using the stochastic finite element method. As the increase of random grain boundary fraction, the fracture performance undergoes three stages. Firstly the fracture energy decreases rapidly. But then it may increase and reach a relatively high level in some range of the random grain boundary fraction. Finally it will degrade slowly. The statistical results also confirm this phenomenon. Two toughening phenomena by random grain boundaries are revealed. The results of the wide band model are similar but the fracture energy is much higher than that of the narrow band model, showing a size effect.

References

[1] Watanabe T. An approach to grain boundary design for strong and ductile polycrystals. Res Mech 1984;11(1):47–84.
[2] Watanabe T, Tsurekawa S. The control of brittleness and development of desirable mechanical properties in polycrystalline systems by grain boundary engineering. Acta Mater 1999;47(15):4171–85.

[3] Chen H-S. Metal's elastic anisotropy. Beijing: Metallurgy Industry Press; 1996.
[4] Dao M, Li M. A micromechanics study on strain-localization-induced fracture initiation in bending using crystal plasticity. Philos Mag A 2001;81(7):1997–2020.
[5] Li J-R, Wang X, Yu J-L. Numerical simulation of deformation localization in coarse-grained aluminum specimens. Acta Metall Sinica 2001;37(7):717–22.
[6] ABAQUS, version 5.8, Hibbitt, Karlsson and Sorensen, Inc., Pawtucket, RI, 1998.
[7] Camacho G-T, Ortiz M. Computational modeling of impact damage in brittle materials. Int J Solids Struct 1996;33(20–22): 2899–938.